Eur. Phys. J. Special Topics **227**, 61–71 (2018)

https://doi.org/10.1140/epjst/e2018-00072-8

THE EUROPEAN PHYSICAL JOURNAL SPECIAL TOPICS

Regular Article

Response of a polystyrene foam subjected to large strains and high pressures

G.R. Johnson[1,a], T.J. Holmquist[1], S. Chocron[2], and N.L. Scott[2]

[1] Southwest Research Institute, Minneapolis, MN 55416, USA
[2] Southwest Research Institute, San Antonio, TX 78228, USA

Received 2 August 2017 / Received in final form 28 December 2017
Published online 10 September 2018

Abstract. This article presents experimental data, and their comprehensive analysis, for a polystyrene foam (with an initial density of $0.623\,g/cm^3$) subjected to large strains and high pressures. The data were obtained from unconfined uniaxial stress tests in compression (at two different strain rates), confined compression tests with compressive strains to almost 50%, and a tension test. The confinement for the compression tests consists of a steel cylinder with external strain gages to monitor the hoop strains due to the radial stresses from the compressed foam. The procedure used to analyze the data allows for a continuous determination of axial, radial and hoop stresses, pressure, and von Mises equivalent stress. A parametric finite element analysis was used to provide for the determination of the stresses from small strains to large strains approaching 50%. There is excellent agreement between test results for similar conditions, as well as the results from data obtained from the confined experiments with two different wall thicknesses. The strength (von Mises equivalent stress) is highly dependent on the pressure, but not as dependent on the strain. The strain rate has a significant effect on strength for the uniaxial stress tests, but only limited data were obtained. Constants were obtained for an existing computational model, and there is good correlation between the experimental data and the model.

1 Introduction

Foam materials are used for a wide range of applications, from low-stress conditions for packaging and shipping, higher-stress conditions for containment of electronic components subjected to high dynamic environments, and very high stress and strain conditions for energy-absorbing applications. Not only is there a wide range of foam materials, but each of the specific materials comes in a range of densities. When dynamic computational analyses are performed on systems that contain foam materials, it is necessary to have appropriate material models and constants to represent the foam, and often these are not available.

During the past two or three decades there have been significant research efforts directed at better understanding the response of foam materials to a wide range of

[a] e-mail: grjohnson@swri.org

loading conditions. On the one extreme, some of these efforts have resulted in very complex models, for a specific material, that require numerous and complex experiments. Often these models are not incorporated into production computer codes, and if they are, the appropriate constants for the user's material of interest are not available. The other extreme is that inappropriate elastic–plastic models are used with approximated constants, but these models do not even allow for some of the most basic characteristic of foam materials. Several comprehensive discussions of the many factors associated with testing and modeling foam materials are provided by Neilson et al. [1], Zhang et al. [2], Jo et al. [3], Sherwood and Frost [4], Song et al. [5] and Doroudiani and Kortschot [6]. More recently, Jeong et al. [7] presented a constitutive model for polyurethane foam with strain rate sensitivity, Ju et al. [8] determined parameters and performed computations for a hyperelastic constitutive model for polyurethane foam, Mouhamadou et al. [9] performed both finite-element and micro-structural modeling of foam materials, Srivastava and Srivastava [10] used two different existing models to investigate the response of Expanded Polypropylene, Goga and Hučko [11] presented a new phenomenological model for foam materials, and Lewis [12] presented a compressible hyperelastic model for foamed rubber.

The work presented in this article is for a polystyrene foam subjected to large strains, high pressures, and a range of strain rates. Data from both confined and unconfined experiments are obtained, and the essential features of the responses are identified and quantified, and put into a relatively simple computational model. The confined experiments are conceptually simple, the analysis techniques are straightforward, and a single test provides data for a wide range of conditions. The remainder of this article provides the experimental results, an analysis of these results, and the determination of constants for a simple computational model.

2 Experimental results

The experiments were performed on a polystyrene foam with a density of $0.623\,\mathrm{g/cm^3}$. The material was obtained from the U.S. Army Armament, Research, Development and Engineering Center (ARDEC), and it was delivered in the form of cylindrical specimens with a diameter of 19.05 mm and a length of 38.1 mm. Most of the tests were performed on the specimens as received, and all of the tests were performed on an MTS servohydraulic load frame.

The data obtained from the compression experiments are shown in Figures 1 and 2, and the test fixture for the confined tests is shown in Figure 3. Some additional data for the hoop strains on the test fixture are provided later. The test fixture in Figure 3 is composed of several steel parts, and the configuration shown is for the thinner sleeve walls (6.35 mm). The strain gage is used to measure the hoop strain in the cylinder such that the radial loading from the compressed cylinder can be determined. The length of the sleeve is 50.8 mm, and the initial length of the cylindrical specimen is 38.1 mm. In the initial condition the sleeve extents 6.35 mm beyond the foam specimen (both top and bottom). When compressed to half the initial length/volume, the sleeve wall extends 25.4 mm above the top of the compressed specimen and 6.35 mm below the bottom of the specimen. The location of the strain gage is at the center of the specimen when it is compressed to half the initial length/volume.

For the unconfined test results in Figure 1 the data are presented as engineering stress versus engineering strain, with compression being positive. Engineering stress for the unconfined tests can lead to errors at larger strains, as the stress is computed from the applied force and the initial area. However, at small strains the stresses

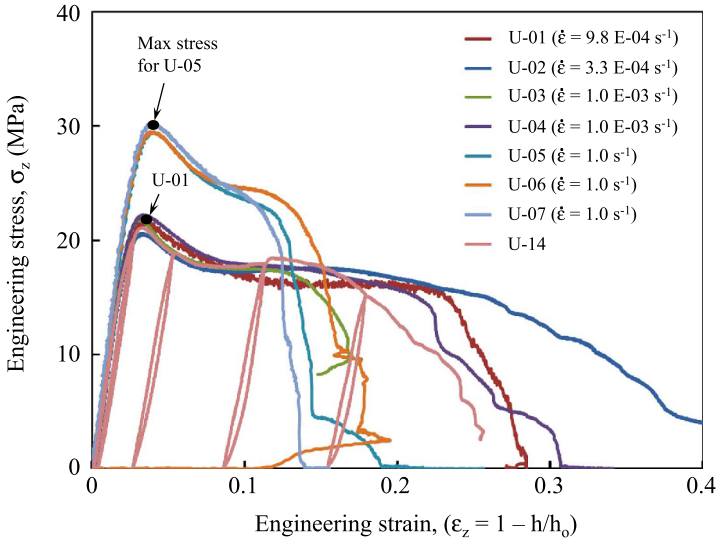

Fig. 1. Engineering stress versus engineering strain for unconfined compression tests at strain rates of $0.001\,\mathrm{s}^{-1}$ and $1.0\,\mathrm{s}^{-1}$.

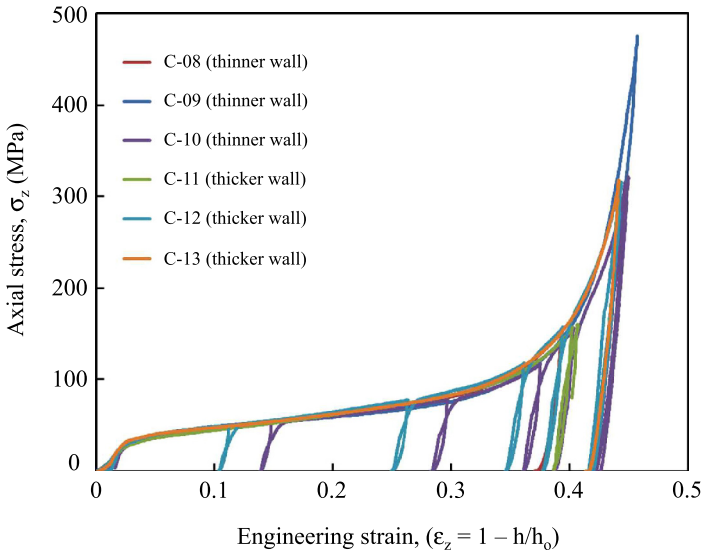

Fig. 2. Axial stress versus engineering strain for confined compression tests at strain rates of $0.001\,\mathrm{s}^{-1}$.

should be accurate. For the confined tests (Fig. 2) the axial stress is essentially identical to the true stress, as the confinement holds the area constant (except for small elastic deformations). The engineering (axial) strain is a value that can be readily measured during the course of the experiments, and it is defined as $\varepsilon_z = 1 - h/h_0$, where h and h_0 represent the deformed and initial lengths of the specimen. The use of confinement to provide higher pressures during testing is not new. Chen and Ravichandran [13] used confinement for split Hopkinson bar tests on sintered aluminum nitride, Forquin et al. [14] used confinement to determine the effect of pressure on concrete, and Chocron et al. [15] used a similar test fixture to determine the effect

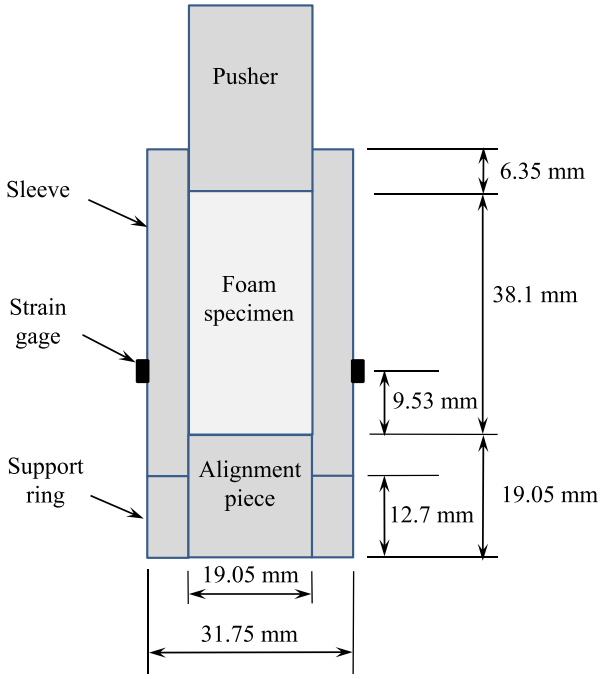

Fig. 3. Test fixture for the confined experiments.

of confinement on predamaged glass. A common requirement is that the strength of the tested material must be significantly lower than the strength of the steel test fixture. The unique feature for this application is that the tested specimen undergoes significant volumetric strains during the course of the test, which provides variable spatial loading on the confinement sleeve.

For the unconfined test results in Figure 1, the data for the lower strain rates ($\dot{\varepsilon} \approx 0.001\,\mathrm{s}^{-1}$) show good reproducibility out to strains of about 0.2, and the data for the higher strain rates ($\dot{\varepsilon} \approx 1.0\,\mathrm{s}^{-1}$) show good reproducibility out to strains of about 0.1. The stresses for the higher-rate tests drop off at lower strains than do the lower-rate results and this is probably because the deformation is not as uniform along the longitudinal axis of the cylindrical test specimen (and failure therefore occurs earlier). It should also be noted that there is sufficient time for numerous wave transmissions throughout the length of the specimen to occur by the time the maximum stresses have been achieved. The maximum compressive stresses for two specific tests (U-01 and U-05) are shown as black dots in Figure 1, and these data are used to determine pressure and strain-rate sensitivity. There is little strain hardening indicated by these data, and the data with strains greater than those indicated by the maximum stresses (which may not be as accurate because of the increased areas of the deformed specimens at large strains) are not used to characterize the response. In fact, there is some strain softening, probably due to damage/pore collapse, that occurs right after the maximum stresses have been achieved.

For all of the tests the specified strain rates are simply the loading velocity divided by the initial length of the specimen (V_{pusher}/h_0). No attempt has been made to compute current strain rates during the duration of the test, or equivalent strain rates, as the differences between the different strain-rate definitions are small when compared to the three decades of strain rates considered (0.001–$1.0\,\mathrm{s}^{-1}$).

Fig. 4. Photograph of the tensile-test configuration and the failed tensile specimen.

The confined test results in Figure 2 are compressed to almost half the initial volume of the cylinders, and then released. Some of the tests include intermediate loading and unloading, but the subsequent responses after the unloading cycles do not significantly alter the responses when compared to the tests which do not including unloading. It appears that the unloading and reloading are elastic responses that do not alter the material. However, it can be seen that the elastic (loading/unloading) stiffnesss tends to increase as the strains are increased. Three of the tests used a test fixture with a thinner sleeve wall (6.35 mm), as shown in Figure 3, and the other three tests used a thicker sleeve wall (9.525 mm). Both fixtures are essentially rigid when compared to the large strains in the compressed foam, and there are no noticeable differences between the data in the two test configurations. There are significant differences in the hoop strains for the two configurations, however, and it is shown later that there is good agreement between the computed stress distributions in the foam specimens.

The tensile-test specimen was machined from the cylindrical specimens noted previously, with a reduced diameter of 12.7 mm in the center. The ends of the specimen (with a full diameter of 19.05 mm) were glued to anvils in the MTS machine with an adhesive. A photograph of the test apparatus and the failed tensile specimen is provided in Figure 4. The tensile stress at failure was 6.7 MPa.

3 Analysis of the confined test results

The data in Figure 2 provide a qualitative indication of the response of the material, but it is of interest to determine the individual stress components, such that a predictive model can be generated to use for other loading conditions. This analysis can be performed by using the axial stress–strain data from Figure 2, together with

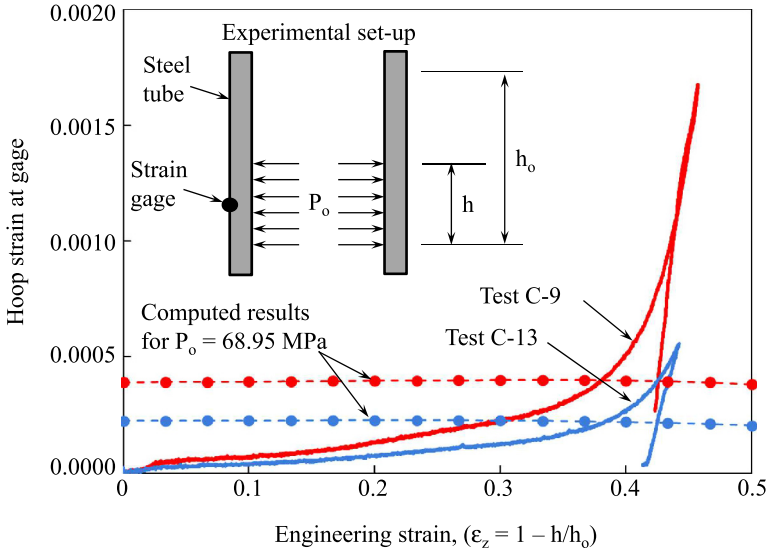

Fig. 5. Hoop strains versus engineering strain in the specimen for experimental results and computed results. Test C-9 has a wall thickness of 6.35 mm and test C-13 has a wall thickness of 9.525 mm.

the hoop strain data shown in Figure 5. The analyses are performed for tests C-9 (thinner wall) and C-13 (thicker wall). As expected, the hoop strains for the thinner wall are greater than the strains for the thicker wall.

In addition to the experimental results in Figure 5, computed results are also shown for a constant radial pressure ($P_0 = 68.95$ MPa) applied on the inside of the steel sleeve. Numerous computations were performed to apply the radial pressure on the sections of the steel sleeve that correspond to the axial strain in the foam specimen. If the length of the foam specimen was always equal to the length of the steel sleeve, then it would not be necessary to perform computations because a simple analytic equation for a thick-walled cylinder could be used. For this application, however, only a portion of the cylinder is loaded and a numerical solution is required. Finite-element computations were performed with the EPIC code [16], using a converged mesh with slowly applied loading (as it is an explicit code). The close agreement with an analytic solution tends to verify the results.

It is interesting that the computed hoop strains are almost constant for the range of applied loadings, and that they are close to the analytic solution. For the thin wall the computed hoop strains vary from 0.000381 to 0.000400, with the analytic hoop strain of 0.000386 (for loading along the entire length of a thick-walled cylinder with no axial load), and for the thick wall the computed hoop strains vary from 0.000204 to 0.000226, with the analytic hoop strain of 0.000229. Due to the design of the test fixture in Figure 3, the only axial load acting on the cylinder is that due to friction between the outside of the foam specimen and the inside of the steel sleeve. The computed and analytic results do not include friction, but it probably does not have a significant contribution to these results. Some support for this assumption is provided by Ilseng et al. [17] who used load cells on either side of a confined rubber specimen, and determined that the frictional effect was less than 1.4%.

With the data from Figure 5 it is possible to determine the radial stress between the foam specimen and the steel sleeve. Because the steel sleeve behaves in a linear elastic manner the radial stress (σ_r) between the two materials, at a given axial strain (ε_z), is simply the applied pressure for the computed strains

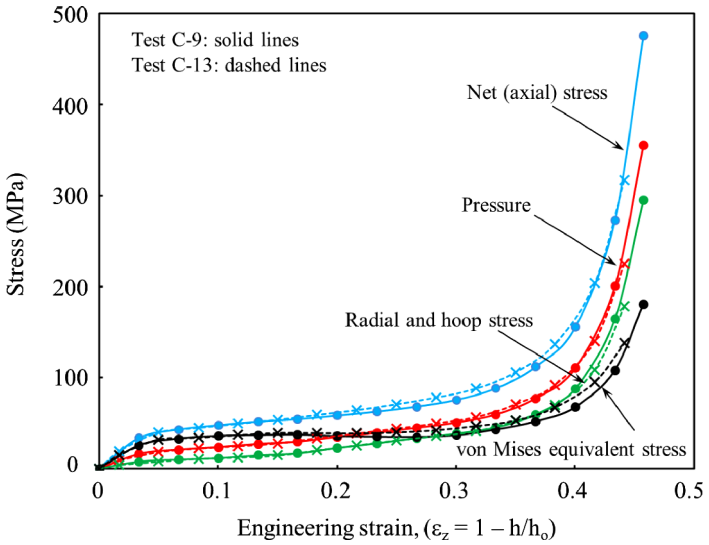

Fig. 6. Stress components for the confined test results. Test C-9 has a wall thickness of 6.35 mm and test C-13 has a wall thickness of 9.525 mm.

($P_0 = 68.95$ MPa), times the ratio of the experimental stress to the computed stress, $[\sigma_r = P_0(\varepsilon_{\text{hoop}}^{\text{test}})/(\varepsilon_{\text{hoop}}^{\text{computed}})]$. After the radial stress is determined the remaining stress components can also be determined. The hoop stress (σ_θ) is equal to the radial stress ($\sigma_\theta = \sigma_r$), the pressure is equal to the average of the three normal stresses $[P = (\sigma_r + \sigma_\theta + \sigma_z)/3]$, and the von Mises equivalent stress (σ) is equal to the stress difference ($\sigma = \sigma_z - \sigma_r$). The results of this analysis are shown in Figure 6. Note that the net (axial) stress (σ_z) is the experimental data from Figure 2, from which the other stress components are computed.

The net (axial) stresses are the experimental stresses from tests C-9 and C-13, and the symbols (dots and crosses) represent the strains (ε_z) at which the other stress components are determined. The unloading stresses are not shown for clarity. The experimental stresses for the two tests are in close agreement, and the other stress components are also in close agreement for the two tests. This is important because the two tests were performed with different test fixtures (thinner and thicker walls) but the analysis procedures provide consistent results – which tends to confirm the approach. It was noted previously that there did not appear to be significant strain hardening for the unconfined tests, and this is confirmed with the von Mises stress changing little under significant strains, between $\varepsilon_z = 0.05$ and $\varepsilon_z = 0.30$. Instead, the von Mises stress appears to be much more dependent on the pressure.

4 Determination of constants for a computational model

It is desirable to put the response into a model such that computations can be performed for a range of conditions. Figure 7 shows an early model for concrete, which was developed by Osborn and incorporated into the Hull code [18]. It is a simple model, but has the features necessary to represent the crushing and pressure-hardening features of the foam considered here. The strength (maximum allowable von Mises stress) is dependent on the pressure and the strain rate, and is bounded by $\sigma_{\max}$. It is not dependent on the equivalent strain. The pressure is represented by

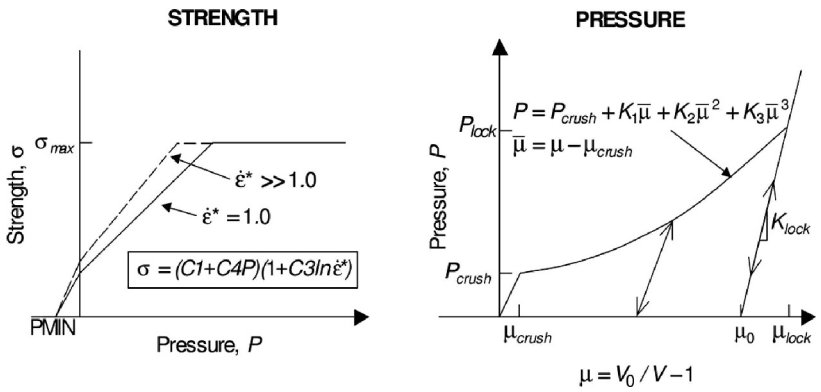

Fig. 7. The Osborn model computational model for crushable materials.

a crushable response. The strain-rate effect for the strength was not included in the original model, but it was subsequently added by the authors. It simply multiplies the pressure-dependent strength by the factor (1 + C3 $\ln\dot{\varepsilon}^*$).

Before the constants are determined for the conditions in Figure 7, the elastic constants can be determined, using the data for $\dot{\varepsilon} \approx 0.001\,\mathrm{s}^{-1}$. The modulus of elasticity is determined from the linear portion of the stress–strain relationship for test U-01, from Figure 1, and it is $E = 870\,\mathrm{MPa}$. The slope of the linear (small strain) portion of the uniaxial strain data for tests C-09 and C-13 (before crushing occurs, as shown in Figs. 2, 5 and 6) is $K + (4/3)G = 1430\,\mathrm{MPa}$, where K is the bulk modulus and G is the shear modulus. K and G can both be expressed as a function of E and ν (Poisson's ratio) and it is possible to solve for ν. The independent elastic constants are then $E = 870\,\mathrm{MPa}$, and $\nu = 0.355$; and the other elastic constants are $G = E/2(1+\nu) = 321\,\mathrm{MPa}$ and $K = E/3(1-2\nu) = 1000\,\mathrm{MPa}$. It is clear from the model in Figure 7 that the bulk modulus can change significantly. The shear modulus may also change, probably bounded by the constant (elastic) shear modulus and a variable shear modulus with a constant Poisson's ratio.

The pressure–volume relationships are shown in Figure 8. Here the volumetric strain is expressed as $\mu = V_0/V - 1 = \rho/\rho_0 - 1$, as this is the definition most commonly used for material models that separate the stress into pressure and deviator-stress components. It can also be determined directly from the engineering strain used to describe the data, where $\mu = \varepsilon_z/(1-\varepsilon_z)$. The constants in the figure correspond to the constants described in Figure 7. K and μ_{lock} are shown as reference values as they can be computed from the other constants. There is a good correlation between the model result and the test data, including the unloading data represented by the square symbols. After the material is compressed beyond μ_{lock} it is confined to the path along K_{lock} as long as the pressure is in compression. The volumetric strain for a solid (non-porous) material (under no pressure) is given by μ_0 and the volumetric strain at which all the voids are crushed out of the material (under pressure) is given by μ_{lock}. Note that μ_0 and μ_{lock} are dependent on one another through K_{lock}. For $\mu_0 = 0.715$ the corresponding density for a solid material is $1.08\,\mathrm{g/cm}^3$, which is close to the handbook values published for solid (non-porous) polystyrene. The minimum pressure (P_{min}) is not shown in this figure, but it is the maximum tensile pressure that can be achieved. It is also used for the determination of the strength under a tensile pressure.

The strength is dependent on the pressure and the strain rate, and a comparison of the test data and the model is provided in Figure 9. The dimensionless strain rate is

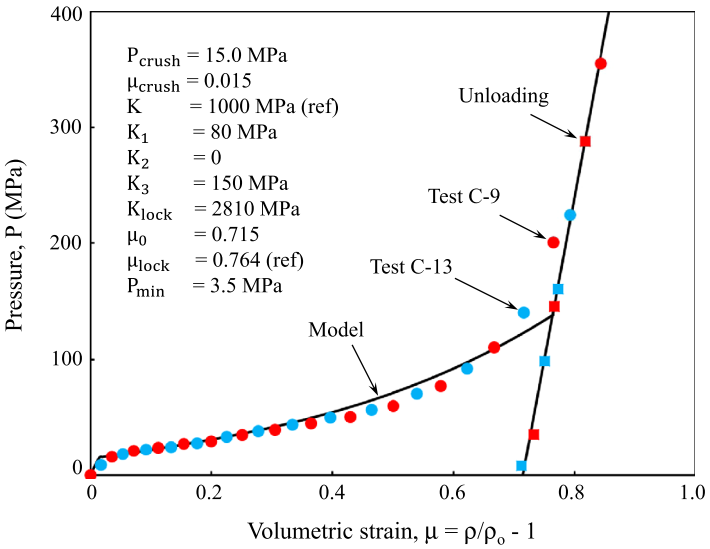

Fig. 8. Pressure–volume relationships for the test data and the computational model.

$\dot{\varepsilon}^* = \dot{\varepsilon}/\dot{\varepsilon_0}$, where $\dot{\varepsilon_0} = 1.0\,\mathrm{s}^{-1}$, and the confined test data are for $\dot{\varepsilon}^* = 0.001$. The maximum stresses for the unconfined compression tests are shown as black dots for $\dot{\varepsilon}^* = 1.0$ (test U-05) and for $\dot{\varepsilon}^* = 0.001$ (test U-01). Again, there is good correlation between the test data and the model, and the strength is highly dependent on the pressure. The strength for negative (tensile) pressure drops linearly from $C_1 = 23.4\,\mathrm{MPa}$ at $P = 0$ to $\sigma = 0$ at $P_{\min} = 3.5$. This is determined from the tensile-test data (test T-01) which provided a tensile strength of 6.7 MPa at a strain rate of $\dot{\varepsilon} \approx 0.001\,\mathrm{s}^{-1}$. Note that a tensile strength of 6.7 MPa has a corresponding pressure of $P = -2.23\,\mathrm{MPa}$, and a straight line through this point (and $\sigma = 18.2\,\mathrm{MPa}$ at $P = 0$ and $\dot{\varepsilon}^* = 0.001$) intercepts the horizontal axis at $-3.5\,\mathrm{MPa}$. Also, the model in Figure 7 allows for a maximum strength ($\sigma_{\max}$) but that is not included here as the test data (for strength) do not appear to level off at the pressures for which test data are available.

A few additional comments regarding the strain rate effects should be made. Generally the pressure–volume relationships for solid materials are not strain rate sensitive. An example is provided by Holmquist and Johnson [19] for silicon carbide, where very similar relationships were obtained from both plate-impact tests (at very high strain rates), and quasi-static diamond-anvil tests. For porous materials, however, this may not be true. The pressure–volume relationships in Figure 8 (especially at low strains with high porosity) may produce higher pressures if the experimental strain rates are increased from the relatively low strain rates ($\dot{\varepsilon} \approx 0.001\,\mathrm{s}^{-1}$) at which they were tested.

Another possible issue is that the strain-rate effects that acted on the unconfined tests (at low pressures) may not have the same effect at high pressures. For a strain rate constant of $C_3 = 0.032$ the strength at a strain rate of $\dot{\varepsilon} \approx 0.001\,\mathrm{s}^{-1}$ is increased by a factor of 1.28 when the strain rate is increased to $\dot{\varepsilon} \approx 1.0\,\mathrm{s}^{-1}$. Even higher factors are experienced at higher strain rates. There is a need for experiments to determine the effects of high strains rates at high pressures.

Some high strain-rate data for a lower-density polystyrene foam ($0.4\,\mathrm{g/cm}^3$) have been reported by Song et al. [5]. These data were obtained with a hydraulically driven test machine for the quasi-static data and a modified split Hopkinson bar apparatus for the higher strain rates, covering a range of 0.001–$950\,\mathrm{s}^{-1}$. Their results did not include confined tests, so the pressures were limited to a third of the maximum axial

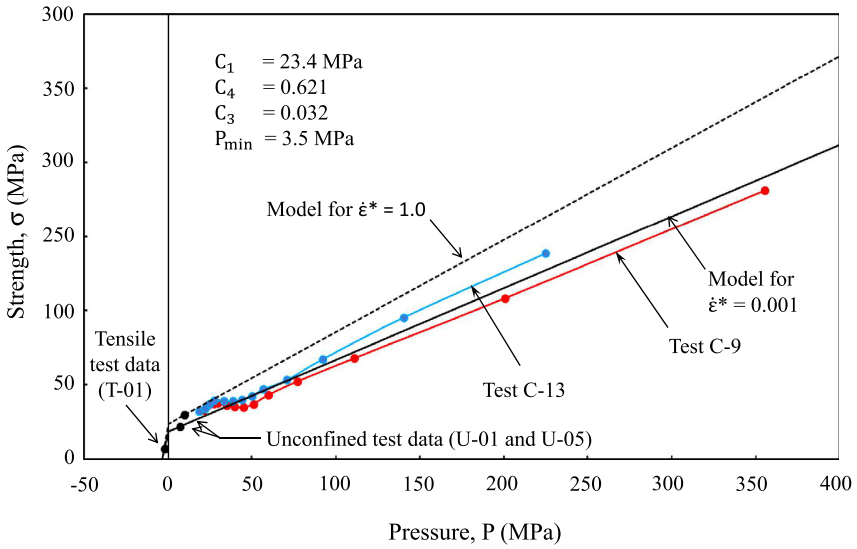

Fig. 9. Strength as a function of pressure and strain rate, for the test data and the computational model.

stresses. Their analysis showed the collapse stress to be expressed as $Y = Y_0 + B$ log $(\dot{\varepsilon}/\dot{\varepsilon_0})$ for $\dot{\varepsilon_0} = 170\,\mathrm{s}^{-1}$. This can be rewritten as $Y = Y_0[1 + (B/Y_0)$ log $(\dot{\varepsilon}/\dot{\varepsilon_0})]$, which has a similar form to the model considered here. For $Y_0 = 14.32$ MPa and $B = 0.64$ [5], and putting their model into the form of the model used here (natural log and $\dot{\varepsilon_0} = 1.0\,\mathrm{s}^{-1}$ as shown in Fig. 7) the equivalent strain-rate constant for the Song et al. data is $C_3 = 0.084$. This is higher than $C_3 = 0.032$ for the present work, but the density and strength of the Song et al. data are significantly lower. Their data also showed the modulus (E) to be strain-rate insensitive up to rates of about $100\,\mathrm{s}^{-1}$, whereas the modulus in the data presented here shows increases at the higher strain rates (Fig. 1). A final comment is that for materials that are both strain-rate dependent and pressure dependent, it is necessary to properly distribute the effects of the strain rates and the pressures. For an unconfined compressive test, for example, a higher strain rate will provide a higher strength. The higher strength also has a higher pressure, and that must be considered. This effect is illustrated in Figure 9. More work is required to determine the effects of strain rates; both for pressure–volume relationships, and strength at combinations of strain rates and pressures. Also, a comprehensive computational model should include the effects of thermal softening and failure, and these effects have not been considered here.

5 Summary and conclusions

This article has presented experimental data for a polystyrene foam subjected to large strains and high pressures. The data were obtained from uniaxial stress tests in compression (at two different strain rates), confined compression tests with compressive strains to almost 50%, and a tension test. The confined test data were analyzed with a technique that allows for a straightforward determination of all of the stress components throughout the entire strain range of the tests. The test data were put into a simple computational model that allows for crushing, loading and unloading,

and strength that is dependent on the pressure and strain-rate; and it was possible to provide a good correlation between the data and the model. Additional work is required to determine strain-rate effects across a range of pressures, and the effects of thermal softening. Damage and failure must also be addressed.

This work was performed under contract W15QKN-14-9-1001 with the Air Force Research Laboratory (AFRL). The funding was provided by the U.S. Army Armament, Research, Development and Engineering Center (ARDEC). The authors appreciate the contributions of Mr Ralph Tatum (AFRL), Dr Jennifer Cordes (ARDEC), and Dr Aisha Haynes (ARDEC).

Author contribution statement

The authors' contributions are as follows: Johnson (50%), Holmquist (25%), Chocron (15%) and Scott (10%).

References

1. M. Neilson, W.-Y. Lu, A. Kraynik, B. Scherzinger, T. Hinnerichs, H. Jin, S. Bauer, S. Hiong, Constitutive models for polyurethane foams, in *Tri-Laboratory Engineeering Conference – 2007. SAND2007-3045C* (2007)
2. J. Zhang, N. Kikuchi, V. Li, A. Yees, G. Husholtz, Int. J. Impact Eng. **21**, 369 (1998)
3. C. Jo, J. Fu, H.E. Naguib, J. Polym. Sci. B: Polym. Phys. **45**, 446 (2007)
4. J.A. Sherwood, C.C. Frost, Polym. Eng. Sci. **32**, 1138 (1992)
5. B. Song, W.W. Chen, S. Dou, N.A. Winfree, J.H. Kang, Int. J. Impact Eng. **31**, 309 (2005)
6. S. Doroudiani, M.T. Kortschot, J. Appl. Polym. Sci. **90**, 1427 (2003)
7. K.W. Jeong, S.S. Cheon, M.B. Munshi, J. Mech. Sci. Technol. **26**, 2033 (2012)
8. M.L. Ju, S. Mezghan, H. Jmal, R. Dupuis, E. Aubry, Cell. Polym. **32**, 21 (2013)
9. D. Mouhamadou, T. Roland, P. Kekicheff, C. Gauthier, Analysis of the mechanical behavior of a polymer foam from 3D full-field strain measurement coupled with finite element modeling at the micro-scale, in *Proceedings 21ème Congrès Français de Mécanique, Bordeaux, France* (2013)
10. V. Srivastava, R. Srivastava, MIT Int. J. Mech. Eng. **4**, 49 (2014)
11. V. Goga, B. Hučko, J. Mech. Eng. **65**, 5 (2015)
12. M. Lewis, Techn. Mech. **36**, 88 (2016)
13. W. Chen, G. Ravichandran, J. Am. Ceram. Soc. **79**, 579 (1996)
14. P. Forquin, A. Arias, R. Zaera, J. Phys. IV **134**, 629 (2006)
15. S. Chocron, J.D. Walker, A.E. Nicholls, K.A. Dannemann, C.E. Anderson, J. Appl. Mech. **75**, 021006-1 (2008)
16. G.R. Johnson, Int. J. Impact Eng. **38**, 456 (2011)
17. A. Ilseng, B. Skallerud II, A. Clausen II, Volumetric compression of HNRB and FKM elastomers, in *Proceedings 9th European Conference on constitutive models for rubber, Prague, Czeck Republic* (2015)
18. D.A. Matuska, R.E. Durret, J.J. Osborn, Hull user guide for three-dimensional linking with EPIC-3, ARBRL-CR-00484 (1982)
19. T.J. Holmquist, G.R. Johnson, J. Appl. Phys. **91**, 5858 (2002)